DOI: 10.1002/adem.200700303

Ferrous Fibre Network Materials for Jet Noise Reduction in Aeroengines Part II: Thermo-Mechanical Stability**

By *J. C. Tan* and *T. W. Clyne**

As outlined in Part I, a promising lightweight material for jet noise attenuation is a highly porous metal, made by bonding metallic fibres into an open network. Results obtained in Part I indicated that major reductions in acoustic intensity, of the order of 5–10 dB in the frequency range of interest (1–10 kHz), are attainable by the introduction of such acoustic modules, without significant penalties in engine thrust or fuel consumption. Stainless steel grade 304 was chosen because of its combination of good high temperature mechanical properties and excellent oxidation resistance (scaling temperature ~ 850 °C).[1] The fibres are produced by melt extraction, a process which is economically attractive and creates fibres with fine microstructure and relatively high strength. Network material is produced by solid-state sintering. There is scope for controlling void content over a relatively wide range (~ 70–95 %). Furthermore, selection of fibre diameter and length, and of consolidation conditions, gives good control over network architecture (distributions of fibre orientation and inter-joint length) and a capacity to generate gradients of structure, which have been shown to have potential for improvement of broadband noise attenuation.[2,3]

[*] *Dr. J. C. Tan, Prof. T. W. Clyne*
Department of Materials Science & Metallurgy
Cambridge University
Pembroke Street, Cambridge CB2 3QZ UK
E-mail: twc10@cam.ac.uk

[**] *Funding for this work has been provided by EPSRC, through a Platform Grant, and by DTI, via a Technology Programme project involving Avcen Ltd and Fibretech Ltd. The authors are grateful to Tom Pomfrett and Kevin Roberts, of the Materials Science Department in Cambridge, who carried out much of the experimental work and provided extensive technical assistance, to Chris Shortall, who provided one of the micrographs (Fig. 4(a)) and to Lee Marston, of Fibretech, who supplied the sintered material and took part in various scientific discussions. In addition, there have been discussions with Dr. Igor Golosnoy, of Cambridge University and Dr. Panos Laskaridis, of Avcen. There has also been valuable input from several members of the committee overseeing the DTI project, notably Prof. Jeff Jupp, Mr. Mike Dacre (Avcen) and Dr. Mike Winstone (DSTL).*

In terms of acoustic performance, the choice of alloy is unimportant (although the network architecture may be significant). However, there are other important aspects to the component performance. In particular, the fibre network module must retain mechanical integrity when subjected to high temperature (~ 650–800 °C) and high velocity gas flows (~ 200–300 ms^{-1}), with superimposed fluctuations and cycles. This is demanding, since such conditions could lead to excessive plasticity, creep deformation and/or fatigue cracking. While it would presumably be possible to replace acoustic damping components at regular intervals, it is clear that rapid gross deformation or damage would be unacceptable. The thermal environment in a jet engine exhaust rules out all polymeric and macromolecular materials, but various metals and ceramics are stable at these temperatures. However, the thermo-mechanical stability requirements generated by exposure to thermal shock, thermal cycling, mechanical vibration and high velocity gas impact are quite demanding. Metals are much more likely to be able to meet these requirements than ceramics. Moreover, while many types of highly porous metal exhibit relatively poor toughness (under tensile loading) and mechanical durability,[4–8] metallic fibre network materials can be relatively strong and tough, provided that the fibre-fibre joints are well bonded together.[9–14] There are techniques available for the manufacture and processing of bonded fibre networks which facilitate the production of strong inter-fibre joints.

The fracture behaviour (tensile strength and fracture energy) of metallic fibre network materials has been relatively little studied. Ducheyne *et al.*[15] measured the tensile strength of sintered 304 stainless steel mats (diameter 50–100 μm), and found it to range up to tens of MPa, as the density was increased up to ~ 40 %. Typically, most steel-based fibre network materials (with relative densities of about 5–20 %) exhibit strengths of a few MPa. Although there have been many studies of the fracture behaviour of thermo-mechanically treated austenitic stainless steels, there are virtually no data available for fibre network materials. Fibre-fibre joint geometry and integrity are likely to be of importance. Experimental studies are needed, since it is very difficult to predict how such joints will behave.

The present paper is focussed on the thermo-mechanical stability of grade 304 fibre network materials, after exposure to high temperatures and high velocity gas streams, for relatively short periods of time. The mechanical integrity is examined by comparing tensile strength and fracture energy data,

before and after isothermal and cyclic exposures. An analytical model is used to predict the network fracture behaviour, using single fibre tensile testing data, combined with fibre orientation distribution data extracted from X-ray microtomography.

Experimental Procedures

Materials

Single Fibres

The stainless steel fibres used were of the Type 304 (Fe-0.08C-19Cr-10Ni-2Mn-0.75Si-0.045P-0.03S), produced by Fibretech Ltd via a melt-extraction route. In this process, a rotating copper wheel, with machined grooves on the surface, is dipped into the surface of a melt. Rapid solidification is initiated on the wheel, and continues in air after the fibres have been ejected from the surface. By varying the aspect ratio of the grooves, either short or continuous fibres can be produced. The melt-extracted fibres used in the present study have a crescent-shaped cross-section, typically with an average diameter of ~ 80–100 μm.

Sintered Network Material

Fibre network materials were produced with relative densities of 5, 10 and 15 %. The fibres were loosely packed in a square die (200 × 200 mm) and gently compacted to obtain the desired densities. The 5 % dense network consisted of longer (~ 20 mm) fibres, while the 10 and 15 % densities were made using shorter (~ 5 mm) fibres. The thickness of the sintered felts ranged from 2.5 to 3.5 mm. Solid-state sintering was performed at 1200 °C for 3 hrs in a vacuum furnace.

The fibre segment orientation distribution in the sintered network was quantified using X-ray microtomography technique, as described by Tan et al.[16] Figure 1 shows the 3D reconstructions of 5, 10 and 15 % densities, and their orientation distributions in both through-thickness (θ) and in-plane (ϕ) directions. It can be seen that all of these materials are transversely isotropic, with the majority of fibre segments lying at $\theta >$ ~ 70°. As the density increases, the probability of segments lying at lower θ angles also rises, as neighbouring segments are more likely to come into contact. The stereographic projections indicate that the ϕ – distributions are approximately isotropic for all densities.

Heat Treatments

Thermal Cycling

Thermal cycling experiments were conducted in a plasma spray facility (Fig. 2(a)). The plasma gun power (15 kW) was chosen so as to generate a plasma plume of similar temperature and gas flow velocity to that in a typical aeroengine exhaust containment region. All tests were carried out in an inert (Ar) atmosphere, in order to minimise oxidation. Strips of network material (150 mm × 20 mm × ~ 3 mm) were attached at both ends to the sample holder. During testing, the plasma plume was traversed in a raster pattern, in order to generate thermal cycles (Fig. 2(b)). The sample front-face and back-face temperatures were continuously monitored, using four K-type thermocouples spot-welded onto the fibre mats. Using this arrangement, the mean temperature of the sample was found to be ~ 700 °C, with a temperature drop of ~ 200 °C through the thickness direction. The gas velocity was ~ 200 ms^{-1}. Each cycling test was conducted for a period of ~ 30 mins. (For the sample geometry employed, these thermo-mechanical test conditions were considerably more severe than typical aeroengine exhaust service conditions.)

Isothermal

The isothermal testing was designed to investigate thermal ageing effects when exposed to elevated temperatures for extended periods of time. Samples were sealed in an evacuated (~ 10^{-3} mbar) glass ampoule and then heat treated at 800 °C for 48 hrs. At the end of the treatment, the sample was slowly cooled to room temperature in the furnace.

Mechanical Testing

Mechanical testing of single fibre and sintered network specimens, in both as-received and as-heat treated conditions, was conducted at room temperature.

Single Fibre Tensile Testing

Mechanical testing of single fibres was performed on a Schenk screw-driven desktop testing machine, fitted with a 250 *N* load cell of ± 0.5 mN sensitivity. Individual fibres (~ 20 mm) were adhesively-bonded onto a pair of paper tabs, with a central cut-out, giving a gauge length of 10 mm. After the tabs were secured in the grips of the testing machine, prior to testing, cuts were made from each side to the central cut-out. All tests were performed at a constant crosshead displacement rate of 0.2 mm min^{-1}. Since the sectional shape of these fibres is crescent-like, the cross-sectional areas (and hence the effective fibre diameters) were estimated by examination of polished sections. The cross-section of a fibre may, however, also vary somewhat along its length. Therefore, at least five samples were tested for each condition.

Network Material Tensile Testing

Tensile tests, of as-received and as-heat treated samples, were conducted using an ESH servo-hydraulic testing machine. The test coupons had dimensions of 150 mm × 20 mm and the mean thickness (~ 3 mm) of the individual specimen was measured using a micrometer. To facilitate gripping, and avoid crushing of the network, both sample ends were impregnated with resin, reducing the effective gauge length to ~ 110 mm. The tensile force was measured via a 10 kN load

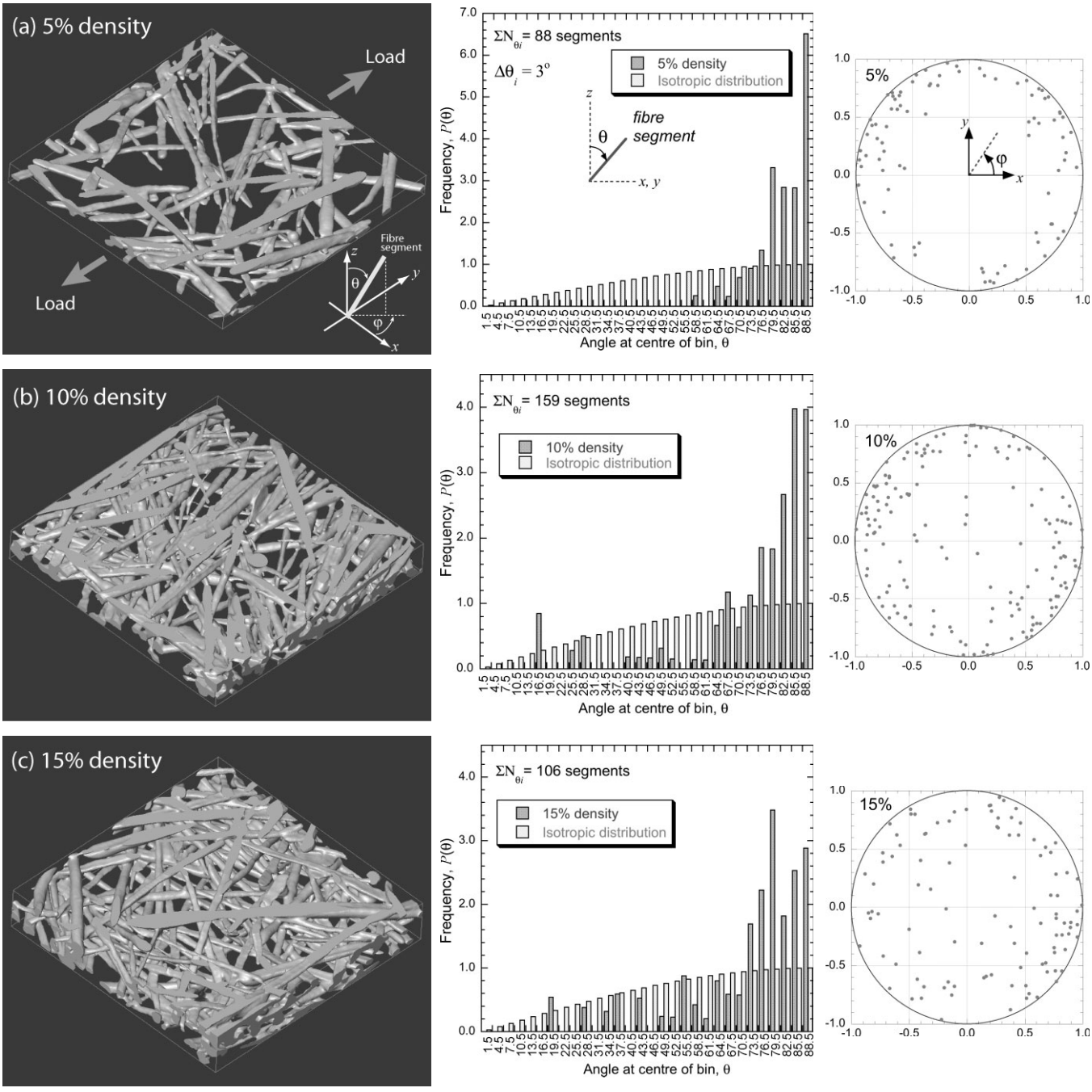

Fig. 1. Fibre architecture information for (a) 5, (b) 10 and (c) 15 % dense networks. The left-hand column shows microtomography visualisations, while the other two columns show fibre orientation data. The central column shows histograms of fibre inclination angle (θ) to the unique (through-thickness) direction, while the right-hand column shows stereographic projections of the in-plane (ϕ) angles.

cell, set to ± 1 kN load range and ± 1 N sensitivity. Due to the highly localised plastic deformation, combined with relatively large strains (≥ ~ 4 %), it was acceptable to obtain the sample extension directly from the crosshead displacement. All tests were performed with a constant crosshead displacement rate of 0.2 mm min^{-1}, until complete fracture. Three to five samples were tested for each condition.

Effect of Heat Treatment on Mechanical Behaviour

Single Fibre Tensile Testing

Stress-Strain Plots

Figure 3 shows representative stress-strain plots for single fibres, before and after the two different treatments. As-received fibres have a yield stress of ~ 800 MPa and a tensile

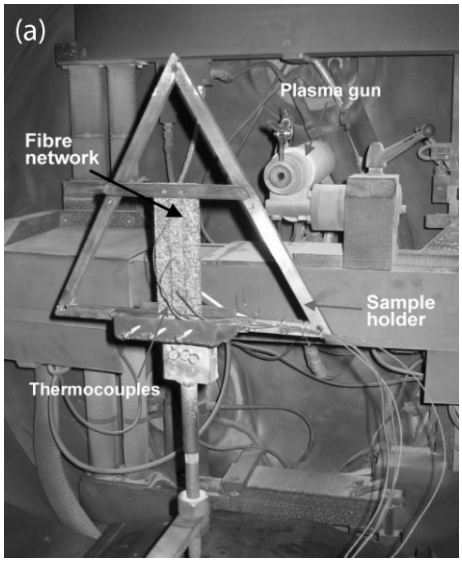

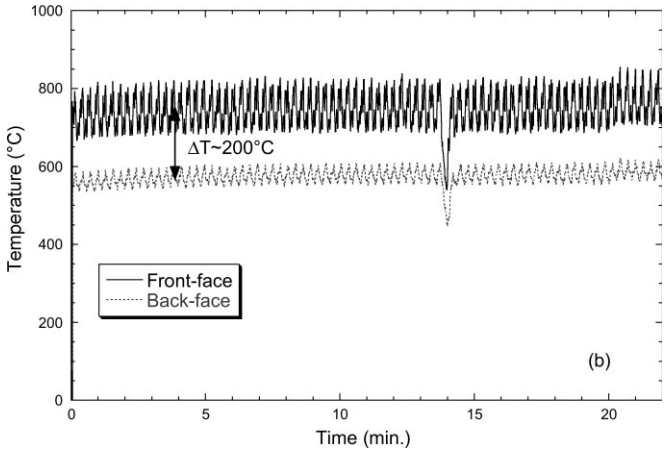

Fig. 2. (a) The thermal cycling setup within the plasma spray chamber and (b) thermal histories obtained from a typical cycling test.

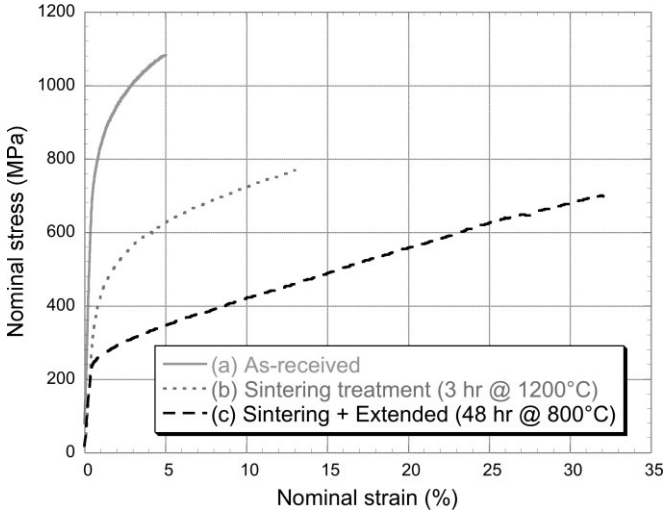

Fig. 3. Representative stress-strain plots for single fibres (a) as-received, (b) after 3 hrs. @ 1200 °C, followed by furnace cooling, and (c) after treatment (b), followed by 48 hrs. @ 800 °C and furnace cooling.

strength of ~ 1 GPa, but the ductility is only ~ 5 %. This is associated with a fine dendritic microstructure (see Figs. 4(a) and 5(a)), and probably a high dislocation density. Fibres heated at 1200 °C for 3 hrs, followed by furnace cooling (ie a similar treatment to that involved in solid-state sintering) exhibited a lower yield stress (~ 400 MPa) and a lower tensile strength (~ 750 MPa). The ductility, however, increased to ~ 12 %. This heat treatment caused substantial grain growth (see Fig. 4(b)) and also a coarsening of the microstructure,

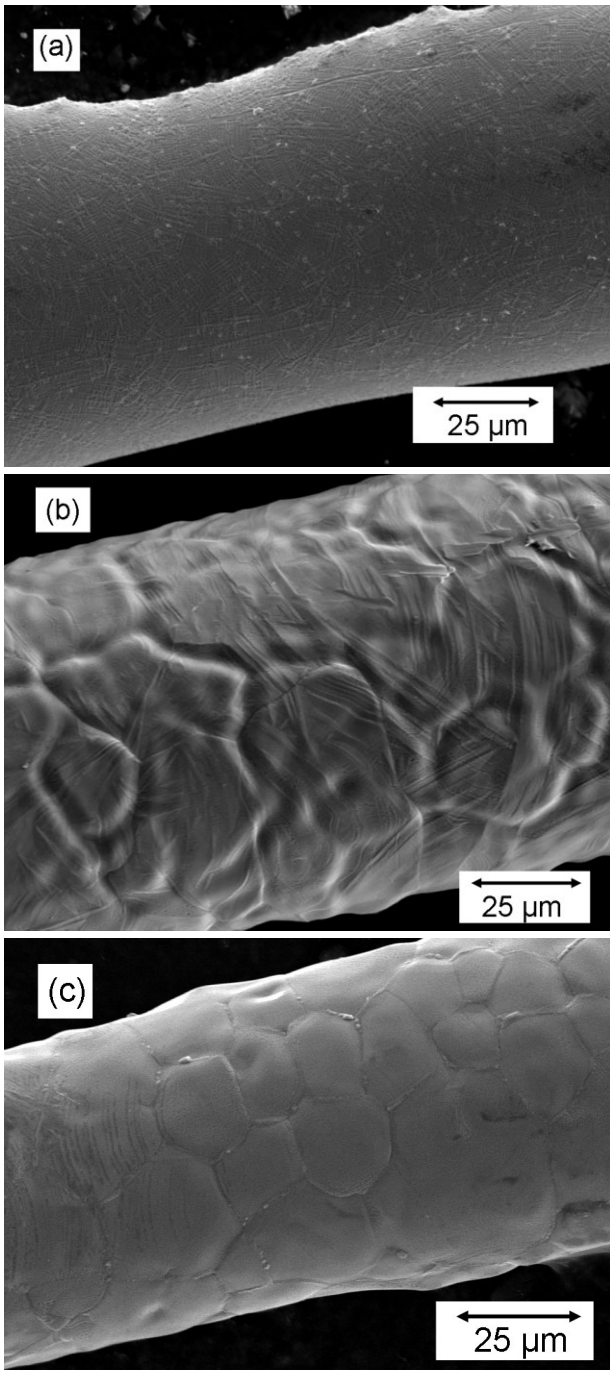

Fig. 4. SEM micrographs of single fibres (a) as-received, (b) after 3 hrs. @ 1200 °C, followed by furnace cooling, and (c) after treatment (b), followed by 48 hrs. @ 800 °C and furnace cooling.

ADVANCED ENGINEERING MATERIALS

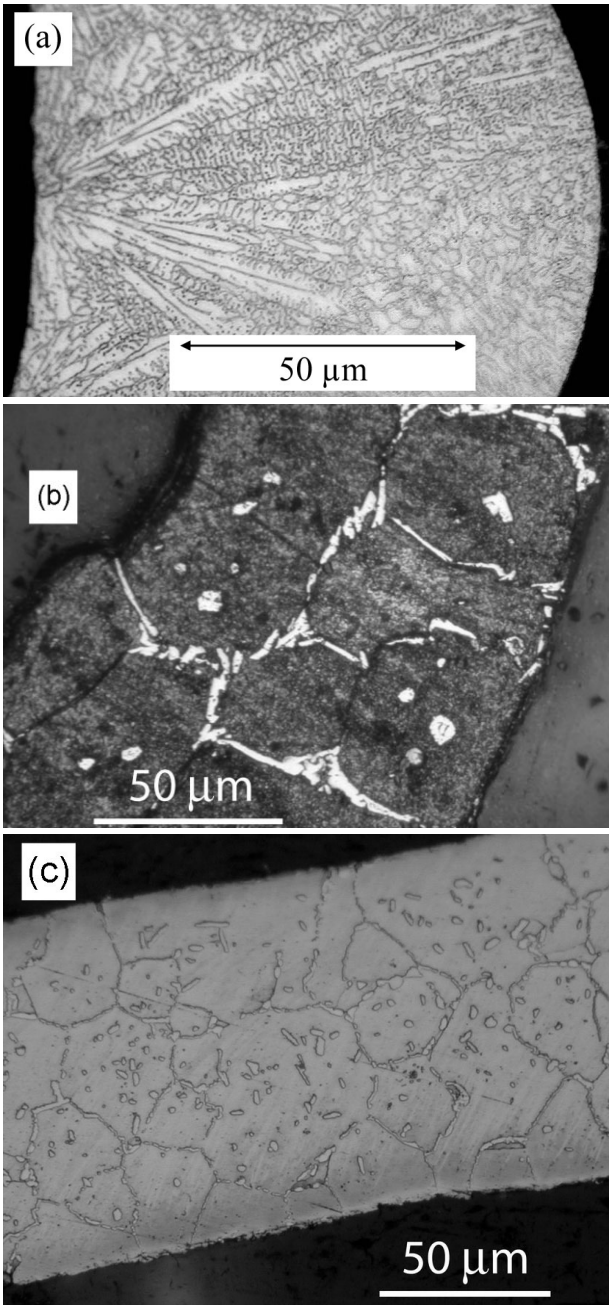

Fig. 5. Optical micrographs of sections through single fibres (a) as-received, (b)after 3 hrs. @ 1200 °C, followed by furnace cooling, and (c) after treatment (b), followed by 48 hrs. @ 800 °C and furnace cooling.

with carbide formation in the grain boundaries (Fig. 5(b)). There will also have been a sharp reduction in dislocation density. Fibres given this heat treatment, followed by 48 hrs at 800 °C, exhibited further strength reductions (yield stress ~ 200 MPa, tensile strength ~ 700 MPa), accompanied by a large increase in ductility (to ~ 30 %). The grain size in this case (Fig. 4(c)) is little different from that after the sintering treatment, but the carbide precipitation is more uniform (Fig. 5(c)), which probably contributed to the higher ductility.

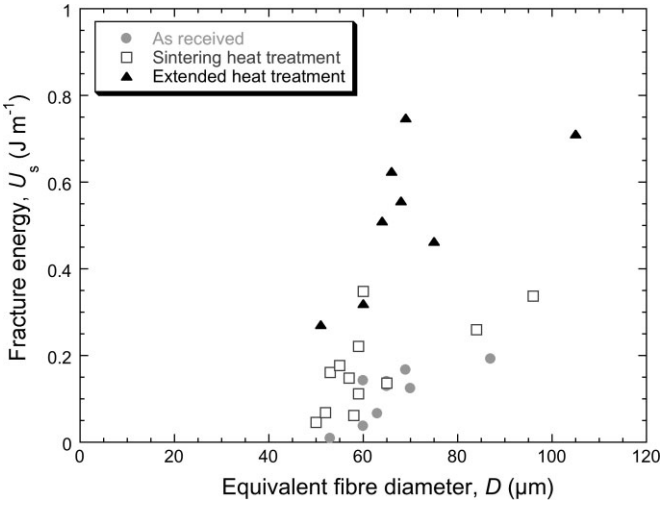

Fig. 6. Fracture energies of single fibres, in different conditions, plotted against the equivalent fibre diameter.

Fracture Energy

Figure 6 shows the fracture energy, U_s (Jm^{-1}), of single fibres, as a function of the equivalent fibre diameter, after different heat treatments. These values were obtained from the areas under plots in the form of load-strain (R vs ε) curves,

$$U_S = \int_0^{\varepsilon_f} P \, \mathrm{d}\varepsilon \qquad (1)$$

where ε_f is the failure strain. This parameter represents the work of fracture of an individual fibre, averaged over the sample (gauge) length. It is used in the model described below. The equivalent fibre diameters ranged from 50 to 100 µm. For a particular heat treatment, it can be seen that there was a tendency towards higher fracture energy for fibres with larger diameters, as expected. As-received fibres have the lowest fracture energies (0.14 ± 0.04 Jm^{-1}), which is attributable to their limited ductility. Fibres subjected to the sintering heat treatment exhibited an improvement in fracture energy (0.21 ± 0.09 Jm^{-1}), due to their higher ductility. Further improvements (0.53 ± 0.17 Jm^{-1}) arose from the extended heat treatment. These changes are attributable to the microstructural changes noted below.

Fibre Network Material

A Simple Model for the Fracture Energy of a Fibre Network Material

A simple way to estimate the work of fracture of a metallic fibre network is to sum the energy needed to plastically deform and rupture all of the fibres in the section, within a process zone of length z. This is illustrated in Figure 7. The concept was introduced by Markaki and Clyne,[17] and is here extended to incorporate factors such as anisotropy. The fracture energy can be expressed as

$$G_{\mathrm{net}} = NU_s z \qquad (2)$$

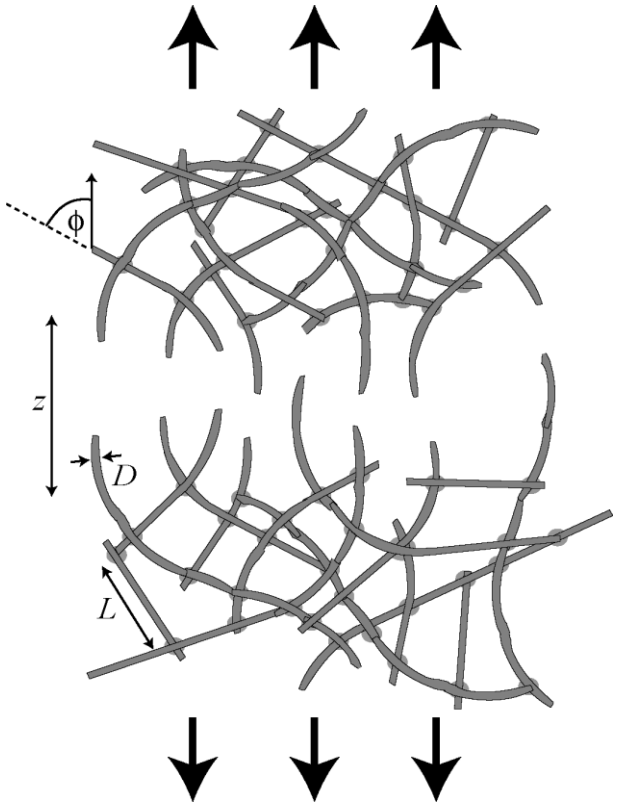

Fig. 7. Schematic of the geometry assumed in the model used for prediction of the fracture energy of fibre network materials. The process zone width is denoted by z, and L is the fibre segment length. The angle ϕ is the in-plane orientation angle, measured from an arbitrary reference direction, taken here as the loading axis.

where N is the number of fibres per unit sectional area and U_s is the single fibre work of fracture, in units of J m^{-1}. The latter is obtained experimentally. Ideally, the single fibre experiments would be carried out on specimens of length z, but in practice the work done during uniform plastic deformation of the whole fibre will often dominate that associated with final necking and rupture (at least for relatively ductile fibres and high aspect ratio fibre segments), in which case this isn't necessary, since U_s will then be independent of specimen length.

The relationship between N and the fibre volume fraction, f, depends on the network architecture. However, if the fibre orientation distribution is isotropic, then an established geometrical result can be used to obtain it. For a set of randomly–oriented prisms, the area intersected by any plane is twice the area intersected by a plane lying normal to the alignment direction of a set of parallel prisms occupying the same volume fraction.[18] Hence, N is half that for an aligned set of cylinders ($=f/(\pi D^2/4)$), ie

$$N = \frac{2f}{\pi D^2} \tag{3}$$

The value of U_s clearly depends on the plastic deformation and rupture characteristics of the fibres. Asssuming that they have yield stress, rupture stress and rupture strain (ductility) values of σ_Y, σ_f and ε_f, and assuming linear work hardening, the work of fracture per unit length can be written as

$$U_s = \frac{1}{2}(\sigma_Y + \sigma_f)\varepsilon_f\left(\frac{\pi D^2}{4}\right) \tag{4}$$

The value of z is likely to fall as the network gets denser. One possible approach is to set it equal to the segment length, L, although it could certainly be larger than this, with an the upper limit presumably being set by the fibre length. If it is to be equated to L, and the material is isotropic, then use can be made of the relationship between L, D and f for a cube array of cylinders

$$f = \frac{3\left(\frac{\pi D^2}{4}\right)L}{L^3} = \frac{3\pi}{4}\left(\frac{D}{L}\right)^2 \tag{5}$$

$$\therefore z = L = \frac{2D}{\sqrt{3\pi f}} \tag{6}$$

Substituting Equations 3, 4 and 6 into Equation 2 gives

$$G_{net} = \frac{2f}{\pi D^2}\left(\frac{\pi D^2}{8}\right)(\sigma_Y + \sigma_f)\varepsilon_f\frac{2D}{\sqrt{3\pi f}} = \left(\frac{\sigma_Y + \sigma_f}{2\sqrt{3\pi}}\right)\varepsilon_f D\sqrt{f} \tag{7}$$

and corresponding predicted plots are shown in Figure 8, for the three sets of single fibre properties of interest here. It can be seen that even low density networks made of these fibres are predicted to have quite respectable fracture energies. Of course, if z turns out to be appreciably greater than L, then larger values are expected for G_{net}.

Effect of Fibre Orientation Distribution

The above treatment (Eq. 7) relates to an isotropic fibre orientation distribution. For anisotropic fibre network architec-

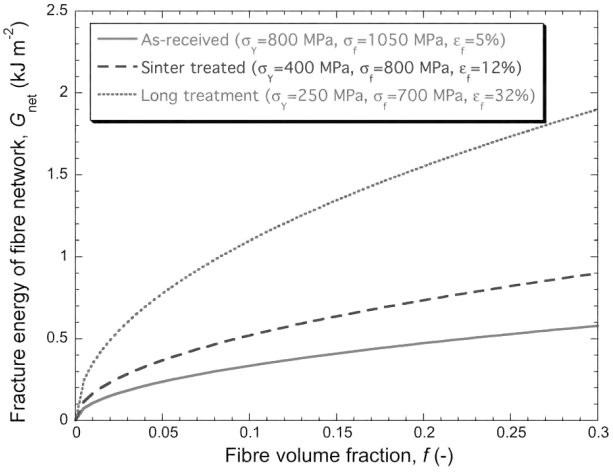

Fig. 8. Predicted plot, obtained using Equation 7, for the fracture energy of isotropic fibre network materials, having the single fibre properties shown (corresponding to the three heat treatments being considered here), and a fibre diameter of 70 μm, as a function of f.

ADVANCED ENGINEERING MATERIALS

ture, the value of N (relation between N and f) will be different. For example, if all of the fibres were inclined at an angle ϕ to the stress axis, then N would be given by

$$N = \frac{4f \sin \phi}{\pi D^2} \tag{8}$$

Of course, this is a rather unlikely distribution. In practice, these materials tend to be transversely isotropic (random ϕ distribution), although they also often exhibit a tendency towards large values of θ (ie for fibres to lie close to in-plane directions) – see Figure 1. However, if the material is being loaded in an in-plane direction, as in the current work, then the distribution of loading angle (ϕ) will be approximately isotropic and there is no need to take account of $\varrho(\theta)$. The use of Equation 3 to relate N, f and D is therefore likely to be acceptable. However, the above relationship (Eq. 5) between f and (L/D) is for a 3-D random orientation distribution and should in general be modified if $R(\theta)$ is anisotropic. In practice, this is only likely to be justifiable if a rather accurate anaylsis is being attempted.

Stress-Strain Plots: Representative stress-strain plots for 5, 10 and 15 % dense sintered fibre networks, in as-received (ie solid-state sintered) and heat treated conditions, are shown in Figure 9. It can be seen that the elastic strains are relatively small (< ~ 0.2 %), compared with the plastic deformation range. The yield point (~ 1 MPa) is not, however, very well defined. The tensile strength is designated as the peak stress, just before the stress level starts to fall rapidly. The accumulation of damage at fibre joints and segments eventually leads to failure, with individual (joint or fibre segment) fracture events detectable as drops in stress (when viewed at high resolution).

It can be seen that, in the as-sintered condition, 5 and 10 % networks show similar tensile strengths (~ 2 MPa), although the ductility of the 5 % material is markedly higher. For the 15 % dense material, there was a significant increase in strength (to ~ 6 MPa). This is presumably conferred by the increasing spatial density of fibre joints (ie constraints). The 10 and 15 % networks have comparable ductilities (5–6 %). It should be noted, however, that the 5 % network was made of longer (20 mm) fibres, whereas the 10 and 15 % networks were made of shorter (5 mm) fibres, and this difference may have contributed to the differences in ductility. Lower volume fractions and longer (initial) fibre lengths translate into longer fibre segments, increasing the degree of freedom at fibre-fibre joints, and allowing more bending and rotational deformation without damaging the joints.

It's also clear that thermal cycling has only minor effects on the mechanical integrity of the 5 and 10 % dense networks. Lower density networks are more compliant, which is expected to make them more strain-tolerant and hence more resistant to thermal shock and thermal cycling effects. The fibre segments in these materials often exhibited ductile fracture behaviour and extensive necking. It may also be noted that the more open architecture of lower density networks will lead to higher permeabilities, reducing the reaction forces imparted by high velocity gases. In contrast, the 15 % dense network, more strongly constrained by fibre-fibre joints, and less permeable, sustained significant damage during thermal cycling. These results are in general consistent with the single fibre tensile testing data, the microstructural observations and the concept that higher network densities will lead to

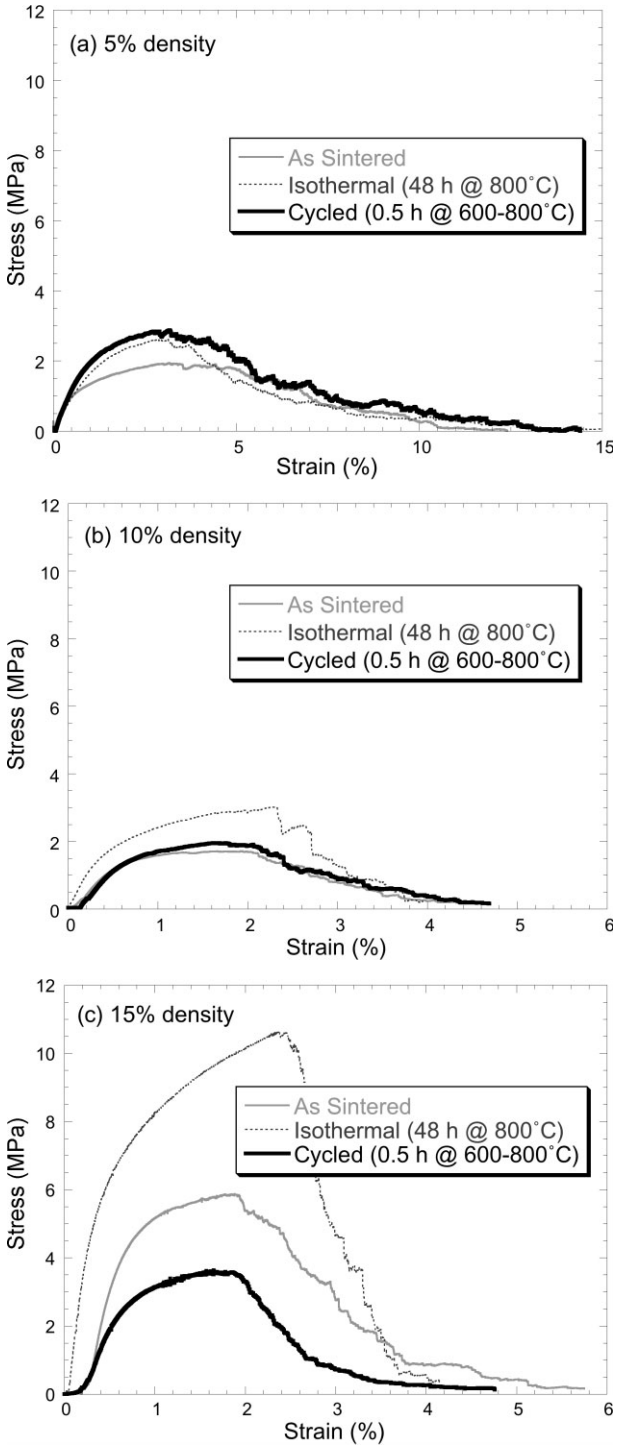

Fig. 9. Representative stress-strain plots for fibre network materials, after different heat treatments, with relative densities of (a) 5 %, (b) 10 % and (c) 15 %.

greater constraint, higher gas-borne forces and reduced strain tolerance.

Fracture Energy

The effects of thermo-mechanical treatment on the measured fracture energy of the network materials are summarised in Figure 10. Data for the fracture energy, G_{net} (Jm^{-2}), were obtained by integrating the area under the stress-displacement (σ vs u) plot

$$G_{net} = \int_0^{u_f} \sigma \, \mathrm{d}u \tag{9}$$

where u_f designates the sample displacement at failure. The relatively high fracture energy exhibited by the 5 % network is apparently associated with its longer (initial) fibre length, which gives rise to high ductility (Fig. 9(a)). It can be seen that the fracture energies of the lower density networks (5 and 10 %) are little affected by thermal cycling, since they exhibit good strain tolerance and hence are more resistant to gas-borne forces. For the 15 % material, however, thermal cycling caused a significant drop in fracture energy, probably due to the development of cracking at fibre-fibre joints (see Fig. 11) as a consequence of the exposure to high velocity gas streams, superimposed with thermal gradient effects. In contrast, there was a clear improvement in its fracture energy after isothermal treatment, consistent with the single fibre test data. This effect, however, was not observed in lower density networks, presumably because they are less constrained.

The values of z shown in Figure 10 were calculated by employing Equations 2–4, using single fibre testing data. The equivalent fibre diameter was taken as 70 μm. The U_s values of individual fibres were taken as those corresponding to the data in Figure 8, which are close to the average measured values for the cases concerned. These predicted z values can be viewed in the light of expected fibre segment lengths in the specimens concerned and also the visual appearance of

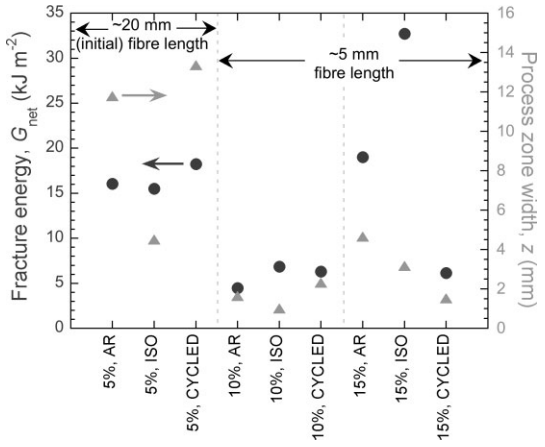

Fig. 10. Average measured fracture energy values for the different fibre network materials, after different heat treatments, and corresponding process zone widths, obtained using Equations 2–4

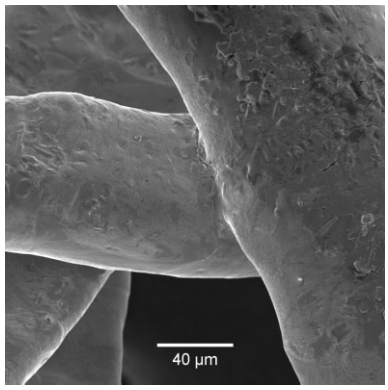

Fig. 11. SEM micrograph of a 15 % density network material, after exposure to the thermal cycling heat treatment, with cracking apparent in the vicinity of fibre-fibre joints.

the specimens after testing. Typical as-tested specimens are shown in Figure 12, for each of the three densities (in the as-sintered state). It can be seen that the predicted values of z for these three specimens, which are respectively of the order of 10, 2 and 3 mm, for the 5, 10 and 15 % densities, are broadly consistent with the process zone widths that could be inferred from the appearance of the specimens (although this is clearly not a precise operation).

On the other hand, it may be noted that these values are rather larger than the fibre segment lengths in these specimens, which are predicted to be appreciably below 1 mm, even for the 5 % density case (L ~ 0.2 mm). This is the reason for the predicted fracture energies in Figure 8 being substan-

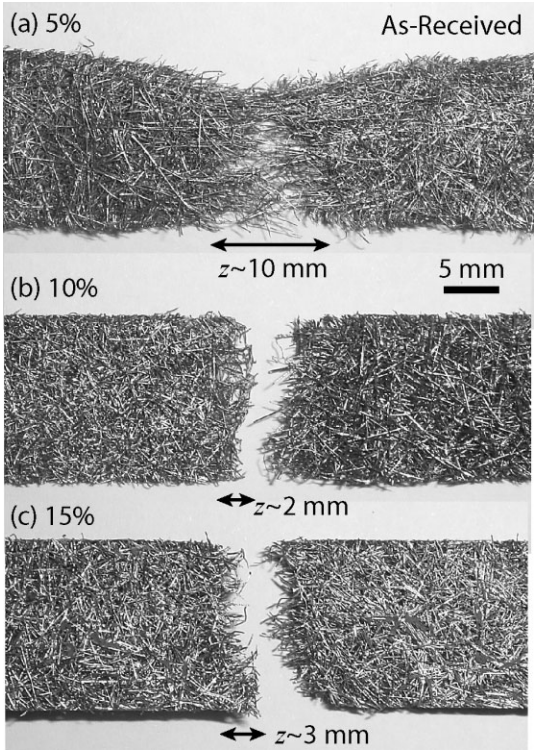

Fig. 12. Optical photographs of fibre network materials after tensile testing.

tially lower than these measured values. It seems likely that the longer fibre length of the 5 % dense material is partly responsible for the relatively large values of z, and indeed it may well be that taking the process zone length as being at least a substantial proportion of the fibre length may be a better approximation than assuming it to be equal to the fibre segment length, at least for the low density networks. Possibly an assumption that it is equal to several segment lengths may be appropriate, but at present this remains an area of some uncertainty.

Conclusions

The following conclusions can be drawn from this work.

An investigation has been carried out into the thermo-mechanical stability of fibre network materials, made by sintering of grade 304 stainless steel fibres. These materials, with relative densities of 5, 10 and 15 %, were subjected to environments similar to those in the exhaust region of a gas turbine aeroengine (ie the impingement of high temperature, high velocity gas streams, generating extended periods at high temperature, thermal shock, thermal cycling and thermal gradients). A study has also been made of how the microstructure and properties of single fibres respond to the thermal histories concerned.

In general, fibre network materials are compliant and strain tolerant, and thus exhibit good resistant to damage under conditions of this type. The fibres do tend to become softer on prolonged exposure to elevated temperature, and in fact the sintering treatment itself also has this effect. However, the main concern is not that the materials should exhibit high strength and hardness, but rather that they should retain their mechanical integrity and shape in the environment concerned. In general, these materials do this very well.

A simple model has been presented for the fracture energy of metallic fibre network materials, which involves the work of fracture per unit length of single fibres and the length of a process zone, within which extensive plastic deformation of the fibres takes place. It is shown that the behaviour of these materials is broadly consistent with this model, with the process zone length being at least several fibre segment lengths. There are indications that a relatively long fibre length may help to maximise the process zone length, at least for relatively low density material. Since the fracture energy is a good measure of the general toughness and damage tolerance, this suggests that it may be advisable to use relatively long fibres in making these materials.

It has been established that materials with up to 10 % density are more compliant and strain tolerant than 15 % dense material. They also appear to be more resistant to thermal shock- and thermal gradient-induced damage. This has been rationalised in terms of the level of constraint imposed on the deformation of individual fibres. It is concluded, in conjunction with the outcome of Part I of this pair of papers, that material with a density of about 10 % appears to offer the best combination of thermo-mechanical stability in the environment concerned and effective acoustic damping properties.

[1] B. Leffler, *Stainless Steels and Their Properties, Avesta Polarit AB, Degerfors,* **2001**.
[2] S. N. Y. Gerges, A. M. Balvedi, *Appl. Acoustics* **1999,** *58*, **403.**
[3] X. Olny, C. Boutin, *J. Acoustical Soc. Am.* **2003**, *114*, 73.
[4] L. J. Gibson, *Ann. Rev. Mater. Sci.* **2000**, *30*, 191.
[5] J. Banhart, *Progress Mater. Sci.* **2001**, *46*, 559.
[6] O. B. Olurin, N. A. Fleck, M. F. Ashby, *Mater. Sci. Eng. A* **2000**, *291*, 136.
[7] C. Motz, R. Pippan, *Acta Mater.* **2002**, *50*, 2013.
[8] Y. Sugimura, J. Meyer, M. Y. He, H. BartSmith, J. Grenstedt, A. G. Evans, *Acta Mater.* **1997**, *45*, 5245.
[9] F. Delannay, T. W. Clyne, in *MetFoam '99*, Verlag MIT Publishing, **1999**, 293.
[10] M. Delincé, F. Delannay, *Acta Mater.* **2004**, *52*, 1013.
[11] F. Delannay, *Int. J. Solids Struct.* **2005**, 2265.
[12] A. E. Markaki, P. Colombo, T. W. Clyne, *Highly Porous Cellul. Met. and Ceram: Thermo-Mech. Properties*, in Encyclopedia of Condensed Matter Physics, Elsevier, Oxford, **2005**, 318.
[13] T. W. Clyne, A. E. Markaki, J. C. Tan, *Comp. Sci. Tech.* **2005**, *65*, 2492.
[14] T. W. Clyne, I. O. Golosnoy, J. C. Tan, A. E. Markaki, *Phil. Trans. Royal Soc. A – Math. Phys. and Eng. Sci.* **2006**, *364*, 125.
[15] P. Ducheyne, E. Aernoudt, P. De Meester, *J. Mater. Sci.* **1978**, *13*, 2650.
[16] J. C. Tan, J. A. Elliott, T. W. Clyne, *Adv. Eng. Mater.* **2006**, *8*, 495.
[17] A. E. Markaki, T. W. Clyne, *Acta Mater.* **2003**, *51*, 1351.
[18] E. E. Underwood, *Quantitative Stereology*, Addison-Wesley Publishing Company, Reading, **1970**.

